aerospace

MDPI

Article

Comparative Study of Composite Delamination Under Quasi-Simultaneous Impacts

Ayoub Soufri [1], Ameur Chettah [1] and Christophe Bouvet [2,*]

[1] Laboratoire DRIVE, Université de Bourgogne, 58000 Nevers, France; ayoub.soufri@segula.fr (A.S.); ameur.chettah@u-bourgogne.fr (A.C.)
[2] Institut Clément Ader, ISAE-SUPAERO, IMT-Mines d'Albi, INSA, CNRS, Université de Toulouse, 31000 Toulouse, France
* Correspondence: christophe.bouvet@isae-supaero.fr

Abstract

This study addresses real-world scenarios such as impacts from hailstones, gravel, or external debris, where multiple simultaneous impacts occur on composite structures. The effects of multiple impacts are analyzed in terms of time lag between impacts, energy levels, and the relative positions of the impacts. Quasi-simultaneous impacts with varying energies are performed, and their results are compared in terms of energy dissipation, delaminated area, and material response. It is observed that, beyond a certain distance between impacts, two simultaneous impacts become equivalent to two mono-impacts. Additionally, a specific energy threshold per projectile exists beyond which the effect of multiple impacts becomes negligible. The findings highlight that the parameter time interval between impacts is the most significant factor in multi-impact studies, unlike in mono-impact scenarios where this parameter does not exist. The study underscores the importance of impact energy, the number of simultaneous impacts and their positions in the evolution of delamination and damage in composite materials. This article provides experimental data on simultaneous multi-impacts that researchers could use to validate their models using a high-complexity problem.

Keywords: quasi-simultaneous impacts; multi-impacts; discrete ply model; delamination

check for updates

Academic Editor: Zhiping Qiu

Received: 5 June 2025
Revised: 9 July 2025
Accepted: 25 July 2025
Published: 27 July 2025

Citation: Soufri, A.; Chettah, A.; Bouvet, C. Comparative Study of Composite Delamination Under Quasi-Simultaneous Impacts. *Aerospace* **2025**, *12*, 669. https://doi.org/10.3390/aerospace12080669

Copyright: © 2025 by the authors. Licensee MDPI, Basel, Switzerland. This article is an open access article distributed under the terms and conditions of the Creative Commons Attribution (CC BY) license (https://creativecommons.org/licenses/by/4.0/).

1. Introduction

Composite materials are frequently subjected to impact loads caused by foreign objects during manufacturing, service, and maintenance operations [1]. Examples of such impacts include road gravel projections during take-off or landing, hailstones, bird strikes, and falling tools during manufacturing or maintenance procedures. The impacts can vary in speed and energy, ranging from low to high, depending on the event [2]. The resulting damage is manifested in various forms, including fiber breakage, matrix cracking, fiber/matrix debonding, and delamination [3]. Due to their limited mechanical properties in the through-thickness direction, composite structures are particularly vulnerable to these foreign impact loads [4].

As a result, the issue of impact-induced damage has been extensively studied in the literature [2,5,6]. However, most studies have focused on cases involving isolated impacts at a single point or repeated impacts [7–9]. In practical scenarios, many structures are exposed to multi-impact loading conditions. Recent research has shifted towards examining multi-impact events, with particular attention given to sequential and simultaneous impacts on

composite structures [4,10–12]. The distinction between these impact types is related to the interaction of stress waves, which can lead to either constructive or destructive interference. An impact is typically classified as simultaneous when stress and shock wave interactions are anticipated [12], and as sequential when the time interval between impacts is sufficiently long to avoid synergistic effects from these interactions [13]. High-energy/velocity impacts on fiberglass composites [4,10,11] or short-fiber reinforced composites [12] are often studied. High-velocity impacts are characterized by very short durations with dilatational wave-dominated responses, while impacts at intermediate velocities exhibit short durations with flexural and shear wave-dominated responses [2].

In multi-impact loading scenarios, the overall structural response is altered compared to single-point impacts due to the activation of more complex damage mechanisms. These mechanisms arise from the interaction of damage induced by different projectiles [4], whether the impacts occur in damaged regions [11] or undamaged regions [12]. The combined effects of crack propagation, stress waves (especially reflected tensile waves), and complex bending effects (which lead to high local tensile stress) have been observed to govern the fracture mechanisms and extent of damage [12].

Paredes-Gordillo et al. [14] aimed to investigate the simultaneous multiple impact response of composite laminates and the effect of stress waves on their mechanical behavior. A numerical model for multiple impacts was developed and validated using experimental data from single impacts found in the literature. It was found that the presence of multiple projectiles reduced the ballistic limit of the composite laminate. The study concluded that stress waves affect the impact response of CFRP plates (carbon-fiber reinforced polymer). The simultaneous multiple impact phenomenon, evaluated with two projectiles spaced twice the projectile diameter apart, showed that stress wave interaction influenced the impact response. This interaction led to material resistance being reached in the impact zones, allowing early perforation by one or both projectiles. A reduction in the ballistic limit was observed in the simultaneous multiple impact (107 m/s) compared to the single impact (118 m/s). The greatest differences in residual velocities were recorded at impact velocities near the ballistic limit (approximately 107 m/s to 180 m/s), with the difference decreasing at higher velocities. As the stress amplitudes increased, material resistance was more easily reached due to the additive effects of stress wave interaction, especially when out-of-plane displacement waves occurred.

An experimental and numerical study by Rezasefat et al. [15] investigates how pre-existing impact damage influences the low-velocity impact response of Carbon Fiber Reinforced Polymer (CFRP). The results indicate that the location of the impact significantly affects the mechanical response and damage to composite skin panels. When the impact location is near the panel boundaries, a notable increase in bending stiffness is observed. Furthermore, pre-existing damage from a 40 J impact at the center of the skin panel results in a more complex impact response, which is dependent on the relative location of the impact to the previous damage. However, when the impact occurs far from the damaged area, no significant difference in response is observed compared to an undamaged specimen.

A review by Kueh et al. [16] discusses recent research on the response of sandwich structures to single and repetitive low-velocity impacts, covering a range of impact energies (0.06–360 J), velocities (0.5–34.2 m/s), and up to 400 repeated impacts. Repetitive impacts, which tend to dominate by indentation, penetration, and perforation, are more destructive as they further compromise the structure's integrity. Despite being more representative of real-world scenarios, repetitive impact behavior has been less studied than single-impact scenarios. It is noted that the energy absorbed plastically decreases with the number of impacts, as the low-energy elements are already damaged, and subsequent impacts affect only those parts requiring higher energy to fail.

The delamination propagation behavior of multidirectional CFRP laminates under multiple indentations was studied by Huo et al. [17]. The study identified delamination link-up as a critical damage feature for multiple indentations, with the delamination growth threshold decreasing at critical interfaces. It was also observed that neighboring damage causes a larger projected delamination area than in cases involving two identical indentations. The study recommends using the cohesive zone model (CZM) to simulate delamination due to ply material degradation. Further research is needed to account for factors such as stress waves, rate sensitivity, and complex loading conditions.

Deka et al. [18] investigated the effects of high-velocity impact on S2-glass/epoxy laminates under both single and multi-site impacts. Their findings show that sequential impacts result in more surface creation than simultaneous impacts. For two and three projectiles, sequential impacts caused 23.0% and 14.2% more delamination damage, respectively, than simultaneous impacts. The interaction between stress waves and delamination damage affected the residual velocity of the projectiles, with the laminate's reduced ability to absorb energy leading to an increased exit velocity.

The response of S2-glass/epoxy balsa core sandwich structures to high-velocity impact was investigated by Vaidya et al. [19], with the study revealing that simultaneous impacts caused more damage compared to single impacts, while the balsa core efficiently absorbed impact energy.

Garzon-Hernandez et al. [20] examined the impact behavior of thermoplastic polymers reinforced with short fibers under single and multi-impact conditions, showing that sequential impacts lead to a reduction in the ballistic limit compared to single impacts. The interaction between cracks, stress waves, and bending effects governed the fracture mechanisms and damage extent.

Jackson et al. [21] conducted an experimental study to investigate the effects of two types of impact damage on the blast performance of sandwich composites. Specimens of sandwich composites were impacted either by a high-velocity projectile or by a low-velocity drop weight. Following the impacts, a secondary blast loading experiment was carried out to assess the influence of the resulting impact damage on the blast performance. The results indicated that damage caused by high-velocity projectiles was predominantly observed on the exit face sheet of the specimens, while minimal damage to the core and the impact face sheet, typically in the form of a hole, was recorded. In contrast, damage from low-velocity drop weights was localized on the impact face sheet and in the core near the impact area. Additionally, debonding between the impact face sheet and the core, along with shear cracking in the core, was observed as a result of low-velocity impacts. Shear cracking in the core was identified as the primary damage mechanism under blast loading. Despite the fact that specimens impacted by high-velocity projectiles absorbed significantly more energy during the impact experiments, the damage caused by low-velocity impacts was found to have the most adverse effect on the blast performance of the sandwich composites.

Bartus [10] uniquely focused on the response of polymer composite materials to impact by multiple high-velocity projectiles. The effects of energy absorption, surface creation, and failure mechanisms from sequential and near-simultaneous multi-site high-velocity impacts were compared to evaluate both synergistic and cumulative effects. It was determined that sequential impacts resulted in 10.1% higher energy absorption and increases of 23.0% (two projectiles) and 10.5% (three projectiles) in delamination damage compared to simultaneous impacts. Cumulative damage was associated with increased energy absorption. While new surface creation did not significantly contribute to energy absorption, its effect on compliance was found to dominate the target response.

Deka et al. [22] aimed to investigate the behavior of laminated composites under high-velocity, multi-site impacts through experimental analysis and finite element model-

ing. High-velocity impact experiments were performed on S-2 glass/epoxy laminates at two projectile locations under simultaneous and sequential impact conditions. While the energy absorption remained relatively constant across the two scenarios, sequential impacts resulted in increased surface creation compared to simultaneous impacts. When projectiles impacted damaged regions, reduced contact stiffness decreased the energy absorption capacity of the laminates, leading to higher exit velocities. This effect was observed in both sequential and simultaneous impacts. Sequential impacts demonstrated a 10.1% higher energy absorption compared to simultaneous impacts, highlighting the distinct response of laminates under varied impact conditions.

Different types of equipment are typically employed for conducting impact tests [23,24]. Commonly used methods include oscillating pendulums (such as Izod [25] and Charpy [26]), falling weights [27], and projectiles launched by gas guns [28]. As the velocity and kinetic energy of the striking mass vary, energy is transferred, and work is applied to the specimen (energy absorption occurs through elastic and plastic deformation, hysteresis effects, friction between the specimen and the test setup, and kinetic energy acquisition by the specimen). To achieve a desired average impact velocity, drop towers, gas guns [28,29], or Hopkinson bars [30], or even universal receiver powder guns, are typically employed. For gas guns, the impact velocity can be varied by adjusting the compressing fluid, the gun's section and length, the mass of the projectile, and the distance between the gun and the specimen. Modern compressed air cannons used for impact testing are designed with key considerations to ensure effective performance. These include optimizing the barrel length and diameter, selecting materials capable of withstanding high pressures, and implementing advanced valve systems to control air release and projectile acceleration. The general configuration of a gas launcher used in high-speed impact tests consists of a pressure vessel, a firing mechanism, a launch unit, a capture chamber, and a velocity measurement unit. Such a cannon is capable of launching a projectile at an initial velocity of up to 700 m/s at a reservoir pressure of 150 bars, with higher velocities achievable when lighter projectiles and higher pressures are employed [11,31,32]. However, these setups typically do not support multi-impact testing, as they cannot simultaneously control the key parameters differentiating configurations, such as the number of impacts, their locations, time delays, velocities, and impact energies.

The behavior of a composite laminate made from unidirectional carbon fibers and an epoxy matrix under multiple medium-speed, medium-energy, multi-site, simultaneous impacts is the focus of this study. A compressed air multi-cannon system was designed and constructed to conduct the multi-impact experiments [33,34]. This setup allows for the simulation of real-service conditions and provides an opportunity to study the structural integrity of composites subjected to simultaneous multi-site impacts. Various parameters, including the number of impacts, their locations, time delays, velocities, and energies, are controlled during these tests.

The effect of quasi-simultaneous impacts has not yet been studied in the literature to assess the interaction between multiple impacts occurring with a time delay shorter than the duration of a single impact. As demonstrated throughout this publication, the most important and influential parameter in a simultaneous impact configuration (with identical energy parameters) is the time delay between impacts. Indeed, two impact configurations involving the same impactors and the same plate do not produce the same delaminated areas depending on whether the impacts are perfectly simultaneous or quasi-simultaneous. It is clear that the literature lacks detailed studies of simultaneous impact configurations, especially in comparing experimental and numerical results across different energy levels, impact locations. Further research is needed to address these gaps in understanding and provide comprehensive insights into multi-impact loading conditions.

2. Materials and Methods

2.1. Materials

Composite laminates were prepared using a draping technique and press-molding of unidirectional carbon fiber/epoxy prepreg with dimensions of 380 mm × 380 mm and a resin content of 37%. The epoxy resin (SE 84LV) was cured using a ramp rate of 2 °C/min, with a minimum viscosity temperature of 99 °C and a dry glass transition temperature of 115 °C. A curing dwell time of 1 h at 80 °C was applied, followed by polymerization under a pressure of 3.5 bar.

High Elongation Carbon (HEC) fibers, with a reinforcement weight of 150 g/m² per ply and a thickness of 0.175 mm, were used. The stacking sequence $[0/-45/90/45]_s$ was adopted, resulting in a planar isotropic laminate. Specimens measuring 350 mm × 350 mm × 1.4 mm were then cut from the cured plates.

For the numerical simulations, the material properties provided by the manufacturer (Gurit [35]) were used as the primary dataset. Missing properties were either supplemented with standard values or extracted from literature sources [36–38]. The utilized properties are summarized in Table 1. The primary objective of the numerical analysis was to investigate phenomena that are experimentally challenging to observe, such as wave propagation and interactions, and to explore variations in impact parameters without requiring repeated experimental campaigns.

Table 1. Material properties.

$\rho_V = 1600 \times 10^{-12}$ tonne/mm^3	(Volumetric mass density)
E_{lt} = 134,000 MPa	(Tensile Young's modulus)
E_{lc} = 121,000 MPa	(Compressive Young's modulus)
E_t = 8300 MPa	(Transverse Young's modulus)
$\nu = 0.3$	(Poisson's ratio)
G_{lt} = 5200 MPa	(Shear modulus in the plane)
$G_{tz} = \frac{E_t}{2(1+\nu)}$	(Shear modulus through thickness)
σ_t^f = 40 MPa	(Transverse failure stress in traction)
τ_{lt}^f = 90 MPa	(Shear failure stress)
σ_0 = 200 MPa	(Crushing stress)
ε_{0t} = 0.0185	(Tensile fiber failure strain)
$\varepsilon_{0c} = -0.0112$	(Compressive fiber failure strain)
G_{Ic} = 0.25 N/mm	(Delamination mode I fracture toughness)
G_{IIc} = 1 N/mm	(Delamination mode II fracture toughness)
$\lambda_{comp} = 0.05$ MPa^{-1}	(Compression reinforcement coefficient)
G_{ft} = 60 N/mm	(Tensile fiber fracture toughness)
G_{fc} = 10 N/mm	(Compressive fiber fracture toughness)
RF = 1,000,000 MPa/mm	(Matrix cracking interface stiffness)

Following curing, specimens with dimensions of 350 × 350 × 1.4 mm^3 were extracted from the 380 mm × 380 mm plates using a diamond bore and subsequently measured to confirm their thickness.

2.2. Methods

The experimental setup consisted of five compressed air cannons, as shown in Figure 1 [33]. The cannon was equipped with an automated triggering system, controlled via a LabVIEW program, to implement the desired shooting configuration.

The setup is presented in our previous work [33], which provides a detailed presentation. A high-speed thermal camera FLIR X6800sc (FLIR LLC, Wilsonville, OR, USA)

captured thermal signatures during impacts, facilitating the reconstruction of damage scenarios and correlation with numerical simulations. Both in-situ and post-mortem damage assessments were conducted.

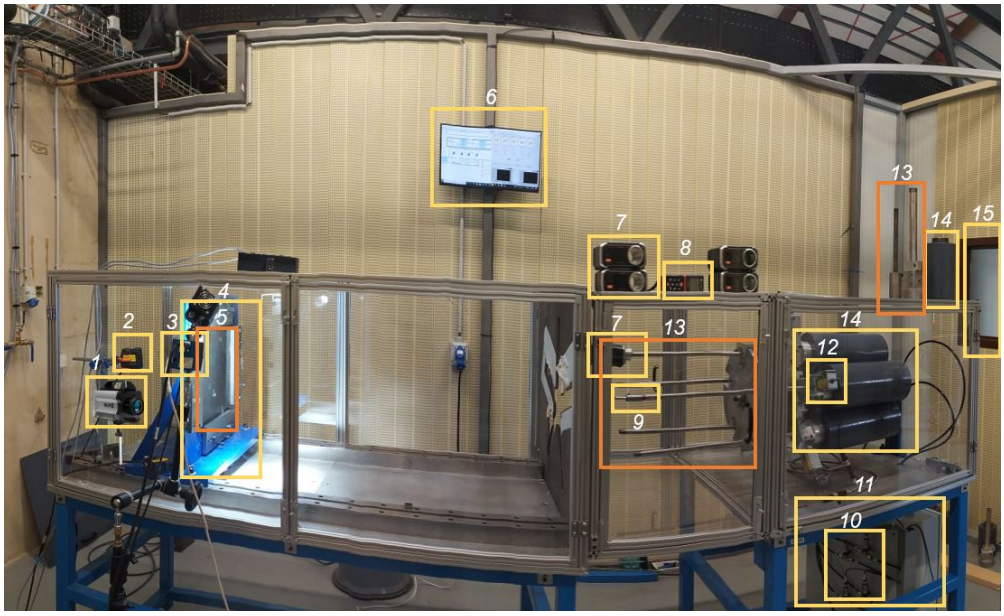

Figure 1. Compressed air cannon test bench: (1) Infrared camera, (2) displacement sensors, (3) high-speed camera, (4) clamping system, (5) composite panel, (6) tv setup, (7) chronographs, (8) laser rangefinder, (9) laser sight, (10) pressure sensors, (11) electrical enclosure, (12) triggering system, (13) guiding tubes, (14) compressed air reservoirs, (15) control room [33].

The velocity of the projectiles exiting the cannon was measured using chronographs Acetech Airsoft Gun AC6000 BT (Acetk Corp Ltd., New Taipei, Taiwan), and high-speed cameras MotionBLITZ EoSens-mini2 (Photon Lines Ltd., Banbury OX16 3ED, UK) recorded pre- and post-impact velocities to determine velocity vectors and the absorbed energy during impacts. Steel balls with a diameter of 20 mm and a weight of 32.7 g were used as impactors.

The composite plate is fixed onto support 4, as shown in Figure 1, and is considered clamped along its edges. The fixation of the plates was verified by conducting several tests to determine the resonance frequencies and modal shapes of a simple structure using the Frequency Response Function (FRF). These parameters were then checked to ensure they remained unchanged after each reinstallation of the plate on the cannon frame. To allow the study of the effect of the distance between two quasi-simultaneous impacts, several configurations with different distances were studied to confirm the trend observed in the results.

Ultrasonic testing (C-scan) in immersion was performed on the manufactured plates to identify potential defects. This process employed a 25 MHz transducer NDT Automation IU25X1-1.5 (MISTRAS GROUP SAS, Sucy-en-Brie, France) and the UltraPAC Immersion Systems device (MISTRAS GROUP SAS, Sucy-en-Brie, France). For analysis, experimental C-scans were compared with numerically simulated C-scans. Among the two measurement types (amplitude and time-of-flight), time-of-flight data was primarily utilized to locate delaminations and validate against numerical models.

Numerical simulations were conducted using the Discrete Ply Model (DPM), initially developed by Bouvet et al. [39] for simulating impacts on composite structures. This model enables the prediction of various types of damage, including delamination, matrix cracking, and fiber breaks, as illustrated in Figure 2.

The DPM operates at the mesoscale (ply-level) and represents plies as strips of volume elements. Zero-thickness cohesive interface elements are introduced between plies to simu-

late delamination. Additional interface elements along the ply length account for matrix cracking. Interactions between inter-laminar and intra-laminar damage are inherently captured by the model. The coupling between these damages is facilitated by information exchange between delamination zones and fiber breakage elements, as well as between matrix cracking zones and matrix damage elements. The numerical model refined the determination of impact times by reprocessing high-speed camera footage for greater precision. It also revealed that displacement sensors should be positioned directly behind impact points to accurately measure local displacement in the impact zone, especially for multiple impacts. Measurements taken far from impact points were found to be less reliable due to wave propagation delays, complicating the interpretation of forces and displacements.

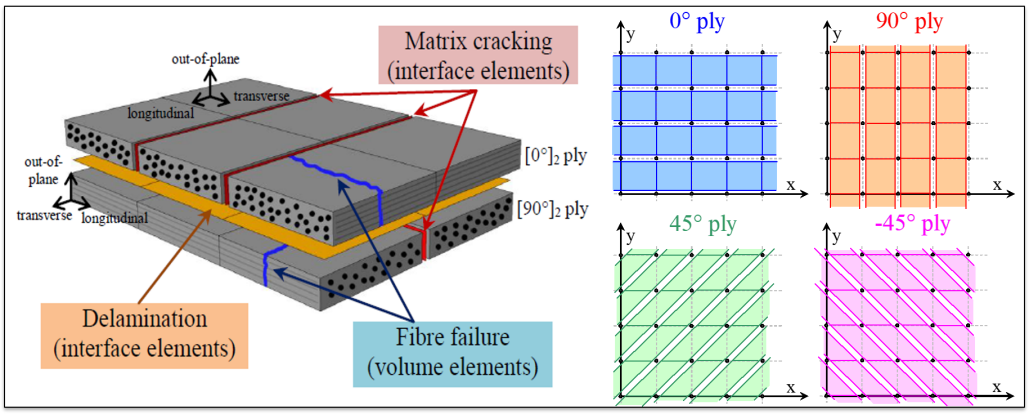

Figure 2. DPM principles and the four mesh types of 0°, 90°, 45°, and −45° plies [39].

3. Results and Discussion

The following nomenclature will be used to distinguish the different configurations tested in this article: "configuration A/B/C", where A specifies the projectile energy in J. B denotes the impact position, explained in a schematic diagram at the beginning of the following sections to distinguish the various possible impact positions, Table 2. C denotes the number of impacts in question. For example, the designation "Configuration 15J/O/2" means that it is a configuration with two simultaneous impacts, each with an energy of 15 J per ball, using 20 mm diameter balls positioned at the O position, as shown in Figure 3.

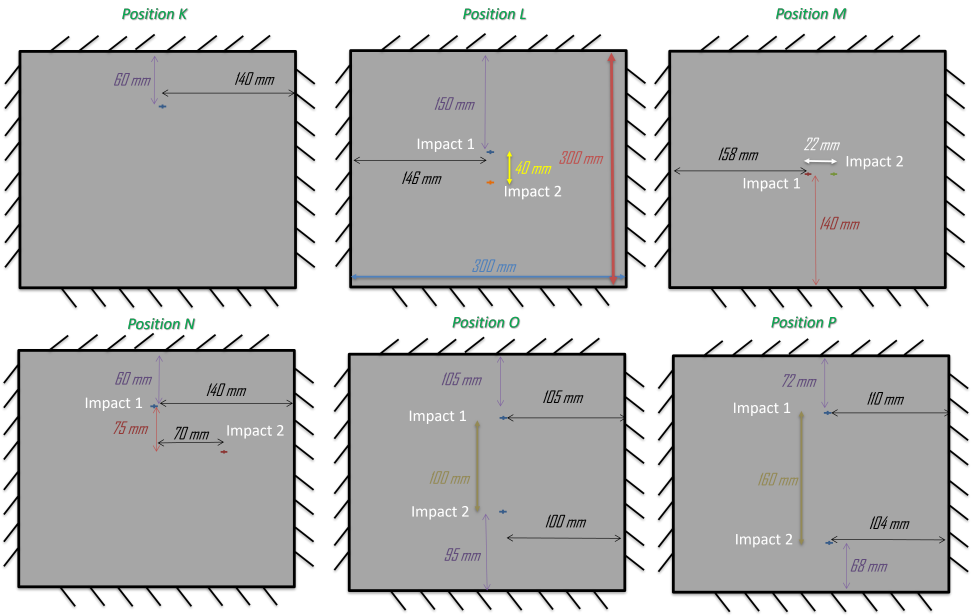

Figure 3. Schematic view of impact positions for each configuration.

3.1. Effect of Distance Between Impacts

To study the effect of the distance between impact centers, particularly in the 90° direction where interference in delaminated areas is not observed, further tests are required in other directions to distinguish between cases with or without overlapping damage zones. In this section, the delaminated surfaces in configurations with two simultaneous impacts at 15 J, using a 20 mm diameter ball, are compared: configuration 30J/K/1 (where the distance between impacts is theoretically 0 mm), configuration 15J/L/2 (where the distance between impacts is 40 mm), configuration 15J/O/2 (where the distance between impacts is 100 mm), and configuration 15J/P/2 (where the distance between impacts is 160 mm). The positions of the impactors are shown in Figure 3.

3.1.1. Mono-Impact Configurations

As shown in Figure 4, each delaminated interface is identified by a number from 1 to 6, starting with 1, which corresponds to the interface between the 0° and −45° plies, labeled as 1:0/−45, and so on (although there are seven interfaces between the eight plies of the composite structure, no delamination is present between the two central 45° plies because they have the same orientation). Each delaminated interface is then marked with a different color, ranging from green on the non-impacted face to dark brown on the impacted face. A scale representing 30 mm is added to each figure to visually assess the delaminated area. The C-scans presented here focus solely on the delaminated zones, as the rest of the plate is not delaminated and therefore shows no color indicating delaminated interfaces.

In order to easily compare the C-scan experimentally obtained with the numerical model, the damaged delamination interfaces ($d > 0.5$) are colored with the color corresponding to the interface color experimentally obtained by ultrasonic investigation. The same procedure has been used for all the comparisons.

In configuration 15J/K/1, the impact is made by a 20 mm diameter ball at an energy of 15 J (velocity of 30 m/s). The average dissipated energy per ball is measured to be 12.92 J, with a standard deviation of 0.06 J, resulting in an average maximum displacement of the impactor of 8.79 mm (with a standard deviation of 0.84 mm), as shown in Figure 4. The model will be presented later. The average impact time in the three trials is found to be approximately one millisecond (the value of the contact time is highly dependent on the acquisition frequency of the high-speed camera). These values are obtained by tracking the ball trajectory with a high-speed camera. In this first case, the C-scan method is used to measure an average delaminated surface area of 653 mm², with a standard deviation of 32 mm². The different interfaces and orientations of the delamination through the thickness can be distinguished.

In configuration 30J/K/1, the 20 mm diameter projectiles are launched with a kinetic energy of impact of 30 J (velocity of 43 m/s). The plates have been perforated, making it difficult to experimentally judge the amount of energy dissipated in the plate. The impact time is measured to be 1.6 ms (compared with 1 ms for the 15 J configurations). However, the plate is not completely perforated: the hole created by the projectile during impact is closed once the ball has pierced the plate. An average delaminated surface area of 4222 mm² is measured, with a standard deviation of 48.54 mm² (Figure 5). The different interfaces and orientations of the delamination within the thickness can be distinguished. All delaminated surfaces are found to be larger compared to the 15 J configurations, especially interface 1, which reaches the edges of the plate. It is important to note that the loss of signal return is related to the chosen synchronization threshold (12%). However, with the same C-scan parameters used in the 15 J configurations, a total loss of signal is observed here due to the breakage of these surfaces, which become too inclined, and the signal return is consequently very weak. It should be noted that the plate is perforated rapidly during impact and then

resealed afterward, thanks to the plies that do not detach due to matrix cracking, which occurs earlier than fiber breakages. Compared to the experiments, the main difference of the DPM simulation is that interface 1 does not delaminate as in real-life conditions. It appears that the fibers are broken precociously and thus stop the delamination propagation. Precise mechanical characterization is required to examine this problem in detail. It should be noted that to make this numerical calculation converge, the broken delamination elements are removed from the model as explained. This abrupt removal of the elements concentrates the stress applied to the fibers and also contributes to their premature destruction.

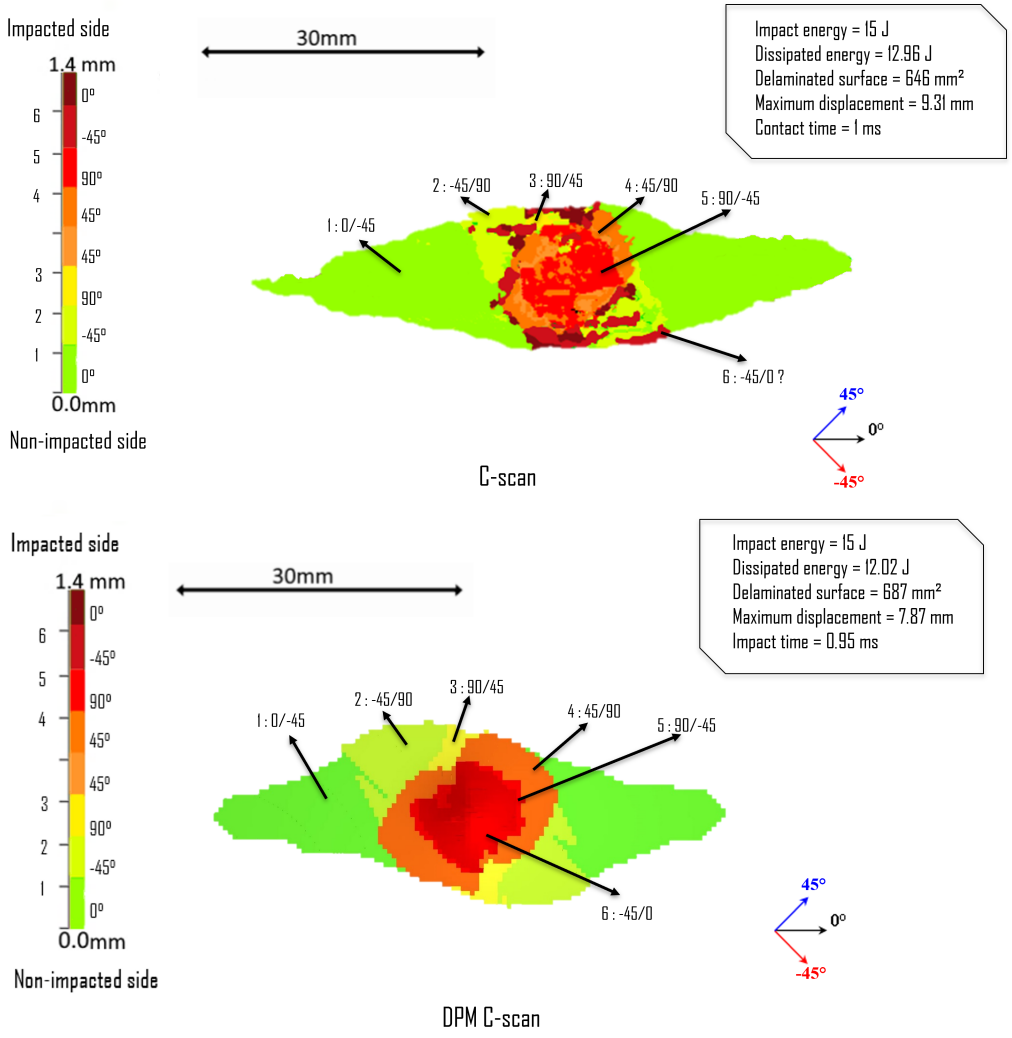

Figure 4. C-scan of a mono-impact (configuration 15J/K/1).

It is noted that the load–displacement curves obtained numerically and experimentally are very similar. For this reason, the model can be relied upon for comparing experimental and numerical tests (see Figure 6). It should be remembered that the experimental curve is derived by twice differentiating the ball displacement curve obtained using the high-speed camera (HSC) [33]. Consequently, all abrupt events (particularly dynamic phenomena caused by the back-and-forth movement of elastic waves, especially those at very high frequencies along the thickness of the plate) are not captured. More detailed insights into the ball-plate contact are provided by the numerical model, with the various force-drop events corresponding to different damage mechanisms. This allows the exploration of other curves obtained numerically to better understand energy dissipation. In Figure 6, the

area shaded in yellow represents the initial kinetic energy of impact. When the ball begins to rebound, its velocity passes through zero at the point of maximum displacement. From that point onward, the ball rebounds (with part of the energy returning to the ball), which is shaded in green in the figure. The difference between these two areas (i.e., the area under the load–displacement curve) primarily corresponds to the energy dissipated due to plate damage, friction, and viscous phenomena, as well as the kinetic and strain energy present in the plate at the end of the contact (represented by blue shading in the figure). This indicates that not all the energy is dissipated within the plate itself. It is verified that the sum of the rebound energy and the so-called "dissipated energy" (in quotation marks because strain and kinetic energy also exist and are not technically dissipated) equals the ball's initial kinetic energy. At the end of the impact, it is observed that in this configuration, less than one-tenth of the kinetic energy is recovered during the ball's rebound. The same work was done for the 15J/K/1 mono-impact. The comparison of the C-scan, experimentally and numerically obtained, is shown Figure 4. The phenomena were experimentally observed, as the direction of the delaminated area by the lower ply direction or the reduced area of the delamination through the thickness was well rendered by the DPM. The simulation of the force–time curve was also created for the 15 J case but is not shown here; more details can be found in [34]. Globally, these good comparisons validate the DPM (except the earlier fiber failure obtained for the 30 J impact, which should be studied farther) and makes it possible to use it to study the simultaneous impacts.

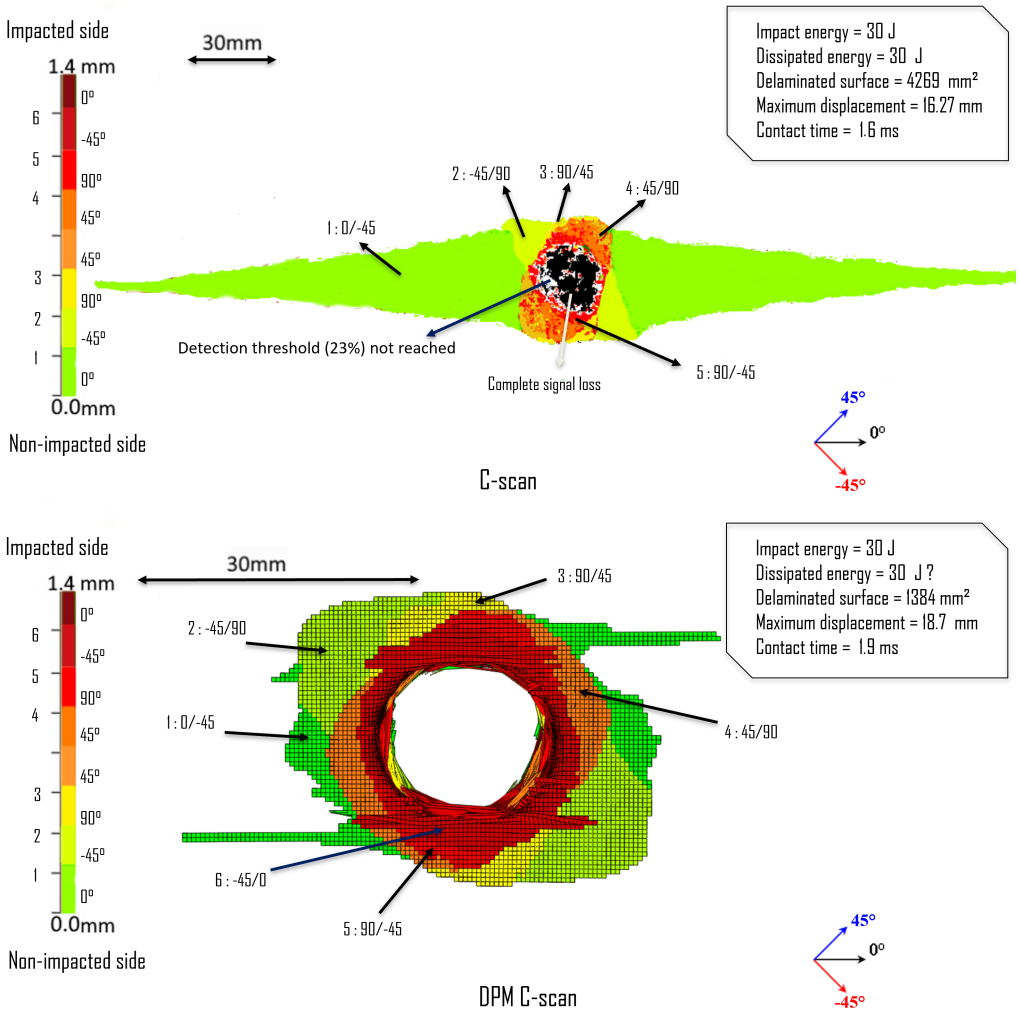

Figure 5. C-scan of configuration 30J/K/1 mono-impact.

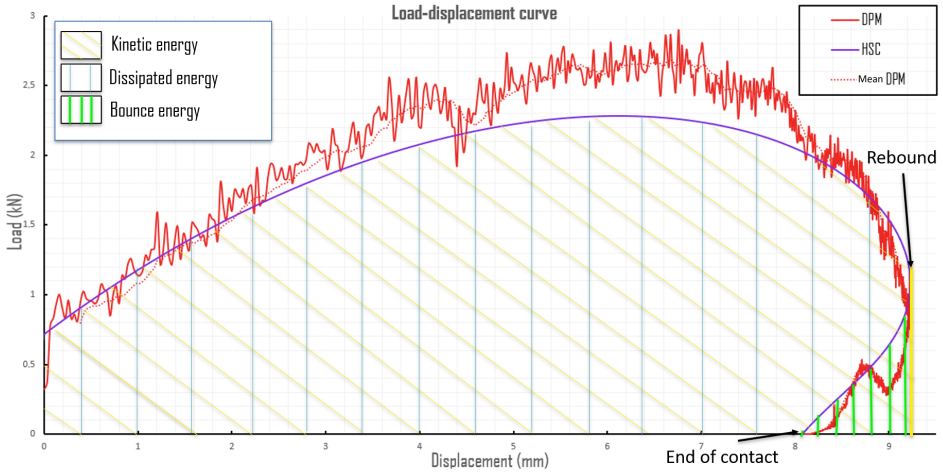

Figure 6. Experimental vs. numerical load–displacement curve of the 30J/K/1 mono-impact configuration.

3.1.2. Configuration 15J/O/2

In this configuration, the distance between the impactors in the 90° direction is 100 mm. The average dissipated energy for the first projectile was measured to be 12.97 J, with a standard deviation of 0.80 J, resulting in an average maximum displacement of the impactor of 7.95 mm (with a standard deviation of 0.17 mm). An average total delaminated surface area of 813 mm² was measured, with a standard deviation of 39 mm² (Figure 7). The average dissipated energy for the second projectile was measured to be 11.63 J, with a standard deviation of 0.11 J, resulting in an average maximum displacement of the impactor of 8.08 mm (with a standard deviation of 0.2 mm). An average total delaminated surface area of 531 mm² was measured, with a standard deviation of 19 mm² (Figure 7). Compared to configuration 15J/M/2 (where the distance between impacts is 22 mm along the x-direction), a 150% smaller total delaminated area was observed in this configuration, Figure 8. This was expected, as the interaction at the delamination level of interface 1 does not occur (since the two impacts are not aligned in the 0° direction). The total delaminated surface is thus the sum of the delaminated areas due to the two impacts, rather than the union of the delaminated surfaces as observed in configuration 15J/M/2. Compared to configuration 15J/L/2 (where the distance between impacts is 40 mm along the y-direction), a 47% smaller total delaminated area was observed in this configuration. This shows that as the distance between impacts increases, the multi-impact effect becomes less significant, as the total delaminated surface is reduced. These experimental results correlate well with the numerical model, as shown in Figures 4 and 7.

3.1.3. Configuration 15J/P/2

In this configuration, the distance between the impactors in the 90° direction is 160 mm. The average dissipated energy for the first projectile was measured to be 12.97 J, with a standard deviation of 0.80 J, resulting in an average maximum displacement of the impactor of 7.95 mm (with a standard deviation of 0.17 mm). An average total delaminated surface area of 813 mm² was measured, with a standard deviation of 39 mm² (Figure 9). The average dissipated energy for the second projectile was measured to be 11.63 J, with a standard deviation of 0.11 J, resulting in an average maximum displacement of the impactor of 8.08 mm (with a standard deviation of 0.2 mm). An average total delaminated surface area of 531 mm² was measured, with a standard deviation of 19 mm² (Figure 9). Compared to configuration 15J/O/2, a 30% smaller delaminated surface was observed, confirming that the greater the distance between impacts, the less significant the multi-impact effect.

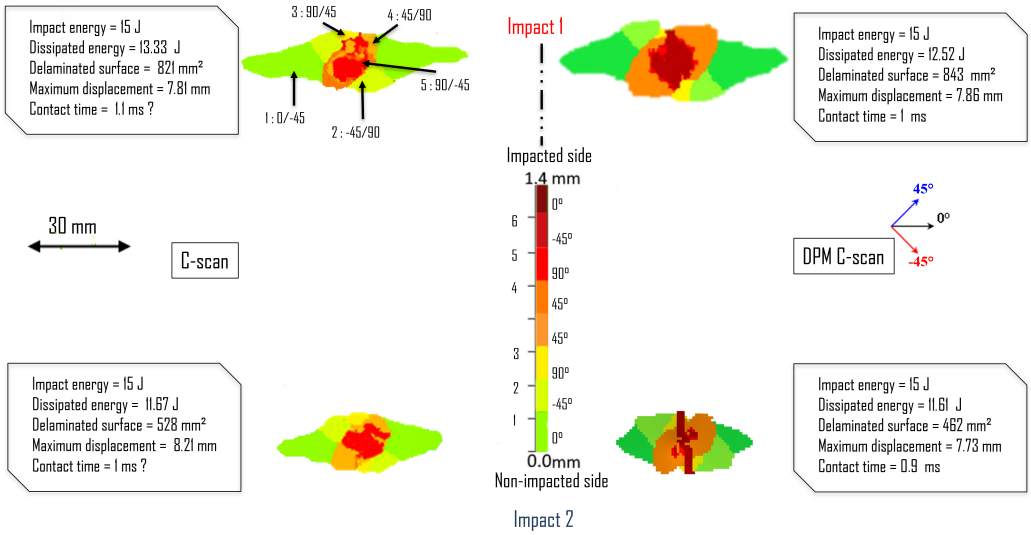

Figure 7. C-scan vs. DPM of the 100 mm distance between impact centers configuration (configuration 15J/O/2).

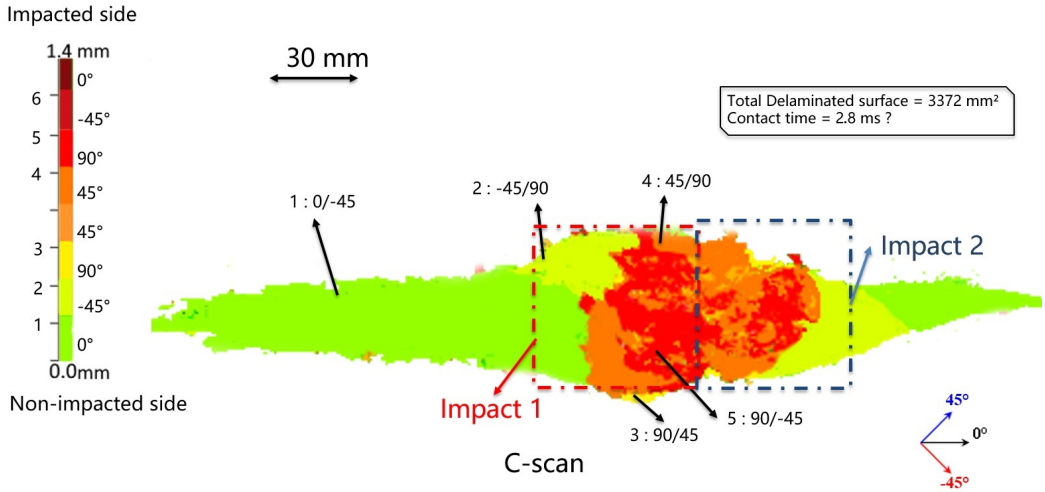

Figure 8. C-scan of configuration 15J/M/2.

The numerical model allows for the observation of the difference in displacement along the *z*-direction of the plate between configuration 15J/L/2 and this configuration, as shown in Figure 10. Displacement is much greater in configuration 15J/L/2, a difference that can be clearly identified at t = 0.6 ms; the C-scan is presented in Figure 11. It should be noted that only the difference in plate vibration between the two configurations is shown here. The greater displacement in configuration 15J/L/2 is not directly associated with the larger delaminated area. In configuration 15J/O/2, the impact is closer to the fixtures, resulting in a smaller tolerated displacement. However, it is evident that neither configuration has reached the displacement limits. In configuration 15J/L/2, an equivalent of 30 J is applied over a smaller area compared to the other configuration, leading to more localized damage.

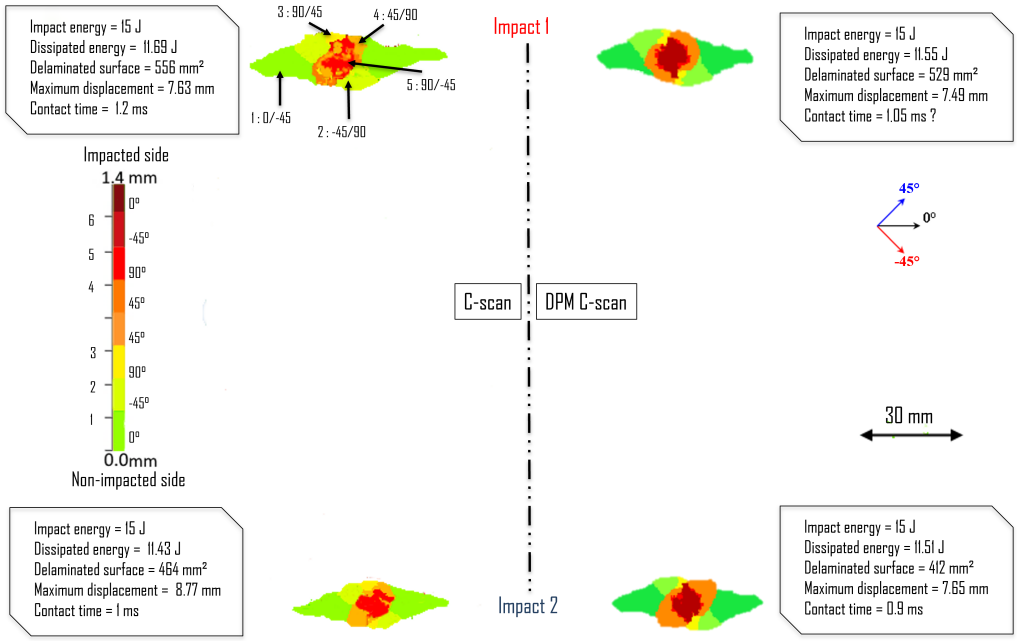

Figure 9. C-scan vs. DPM of the 160 mm distance between impact centers configuration (configuration 15J/P/2).

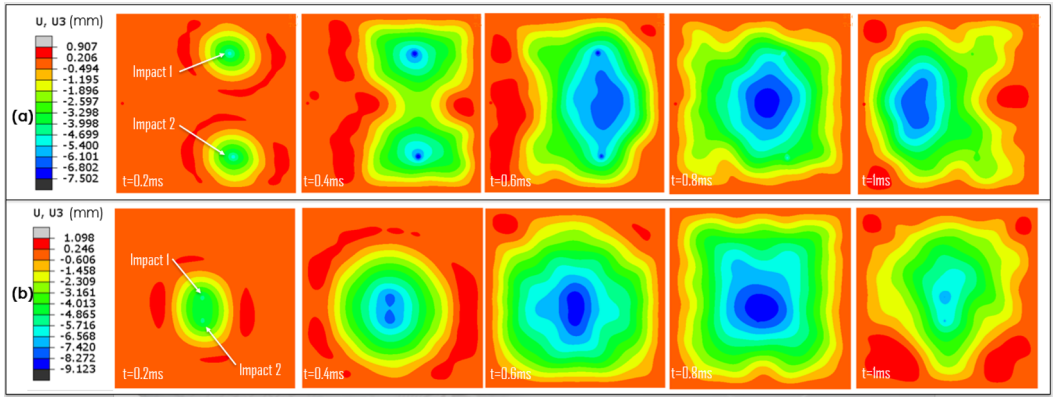

Figure 10. *z*-displacement: (**a**) configuration 15J/P/2, (**b**) configuration 15J/L/2.

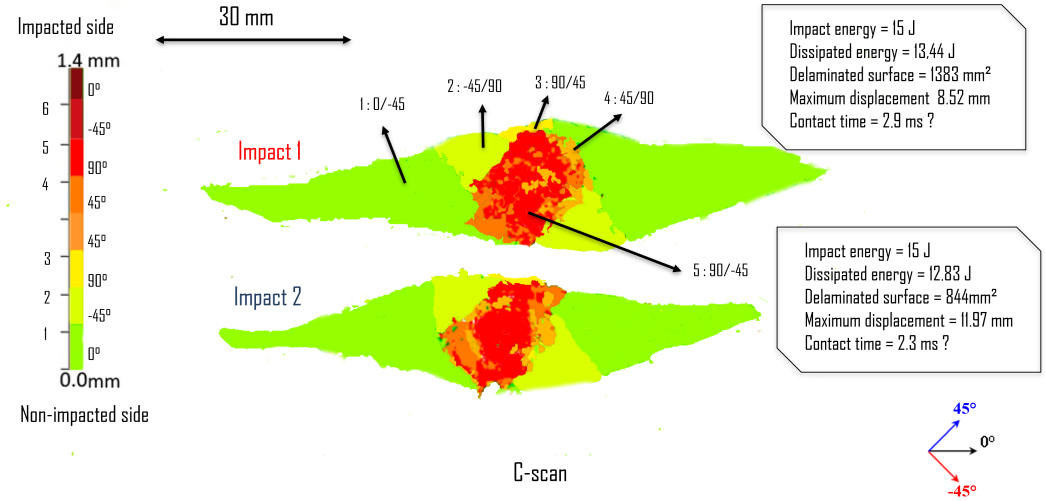

Figure 11. C-scan of configuration 15J/L/2.

In conclusion, it is confirmed that the greater the distance between impacts, the more the configuration tends towards a single-impact configuration. Two simultaneous impacts are equivalent to two times a single impact, as shown in Figure 12, which shows the total delaminated surface as a function of the max distance in x and y between impact points for several configurations of single impacts and two simultaneous impacts at different positions. The smaller the distance between impacts, the more energy is dissipated locally, and the greater the resulting damage. Nevertheless, this result should be taken with caution because the delaminated area is mainly due to the interface 1, and of course, the repartition of the delaminated interfaces through the thickness should be different. This is true except in the case of an offset in the 0° direction, where it becomes important to differentiate between interfered and non-interfered damage zones. If interference occurs, a union of the delaminated interface 1 is expected, which will reduce the size of the delaminated zone compared to another configuration without interference from nearby delaminated zones.

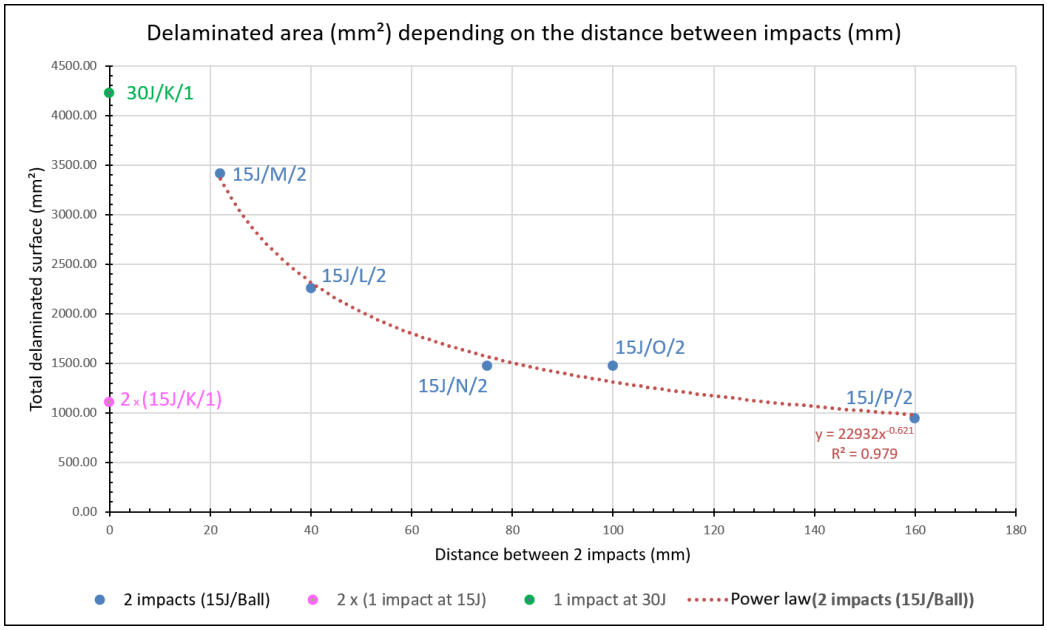

Figure 12. Delaminated area vs. the distance between impact centers.

In this case, from 160 mm between impact centers, the multi-impact effect does not play a significant role compared to a single impact (although it is slightly less than (2 × mono-impact), the difference is not significant due to uncertainties). It should be noted that this result depends on various factors, including impact energy, projectile mass and velocity, material properties, stacking sequence, plate thickness, and shape.

The configuration 15J/N/2 (with a 102 mm distance between impacts, 70 mm along x and 75 mm along y) confirms that these conclusions are valid for directions other than 90°, as it introduces a case with a 22 mm distance between impact centers along the x-direction (15J/M/2). The results of the 15J/N/2 configuration are plotted in Figure 12 as a function of the greatest distance between the x-direction and y-direction, to study the effect in one of the two directions. However, it seems that regardless of the choice for this configuration, the same power law will almost always be followed (see Figure 12), similar to other configurations where the offset occurs only in the 90° direction. Additionally, the delaminated surface in the 100 mm case (15J/O/2) is comparable to the other configuration with 100 mm distance between impacts (15J/N/2), which supports the assumption that distance plays the same role in all directions in configurations without interfering with damaged zones.

It can also be observed in Figure 12 that, from 160 mm onwards (with the parameters of our tests), two simultaneous impacts (15J/P/2) generate the same total delaminated area as two separate single impacts (2 × 15J/K/1). This indicates that there is a threshold beyond which the structure responds similarly to single and multiple impacts in terms of delamination. As a perspective, further investigation is required into other forms of damage, particularly fiber breakage and residual strength.

3.2. Simultaneous Impacts: Effect of Time Lag

It was observed during the research that, with the same impact parameters, the delaminated surfaces differ depending on the time lag between impacts, even in a simultaneous impacts configuration. As shown in Figure 13, in configuration 15J/N/2, for the same energy, velocity, projectile size, and distance between impacts, the delaminated surface is influenced by the time difference between impacts (in Figure 12, Δt_c is equal to 0.1 ms).

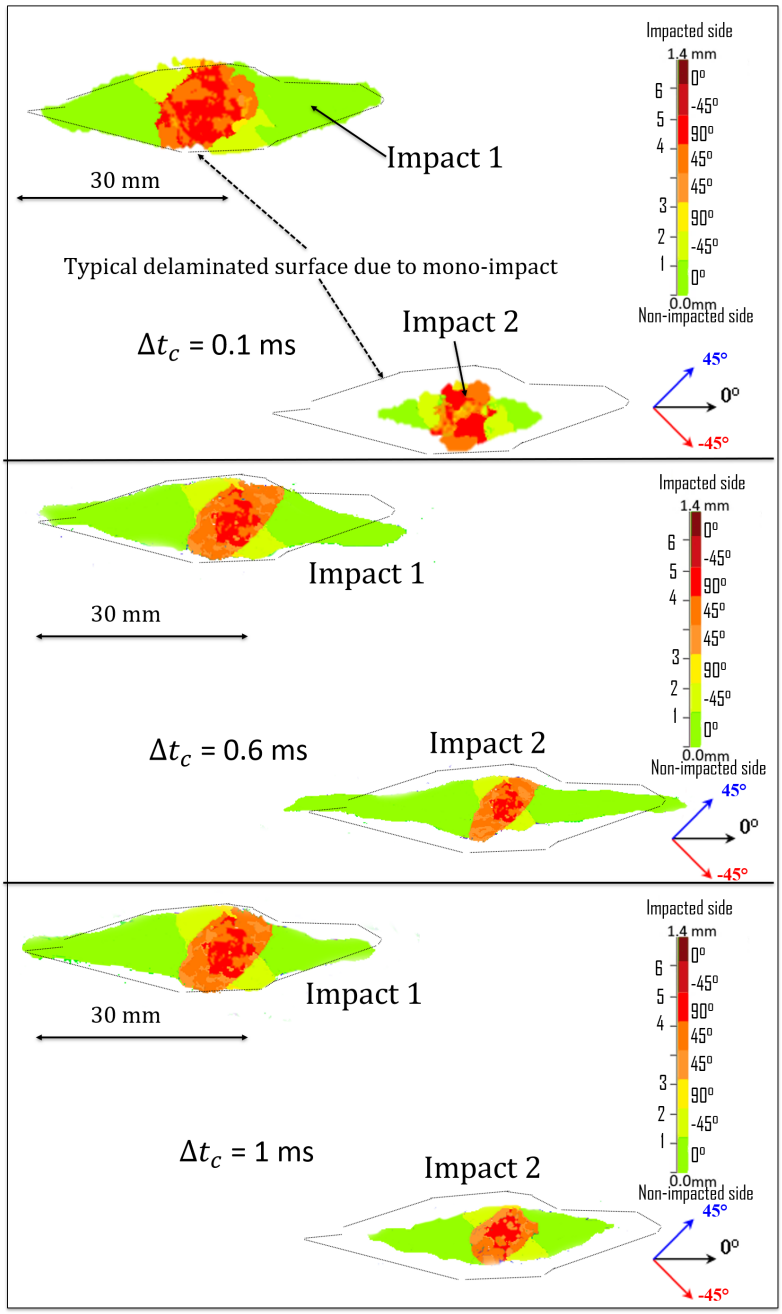

Figure 13. Effect of time lag on delaminated area (C-scan), 15J/N/2.

Table 2. Summary of studied configurations.

Configuration	Figure Reference	Variables
15J/K/1	Figure 4	Energy (single impact)
30J/K/1	Figure 5	Energy (single impact)
15J/L/2	Figure 11	Distance between 2 quasi-simultaneous impacts
15J/M/2	Figure 8	Distance between 2 quasi-simultaneous impacts
15J/N/2	Figure 13	Time lag between 2 quasi-simultaneous impacts
15J/O/2	Figure 7	Distance between 2 quasi-simultaneous impacts
15J/P/2	Figure 9	Distance between 2 quasi-simultaneous impacts

To better understand the reason, the numerical model was used to track the phenomena involved. Initially, the two projectiles are placed at the same distance from the plate. The time difference at the beginning of contact between the projectile and the plate is denoted as Δt_c, as shown in Figure 14. In this figure, the curves of the force–time and displacement–time at the two impact points are also plotted. It makes it possible to highlight the effect of the displacement obtained at an impact point on the impact damage at the moment of the impact beginning. For example, it was noted that at a time lag of 0.21 ms (which is close to the maximum deformation state in the case of a single impact), a very large delaminated surface is generated by the second impactor, as shown in Figure 15. (It should be noted in this figure that inadequate consideration of fiber failure by the DPM could distort the delamination simulation, and this point will be further developed in the next paragraphs). This is identified as constructive damage, where the displacement of the second impactor is added (in the same direction [-*z*]) to that created by the first impactor. In contrast, at 1.45 ms, when the plate is no longer in contact with the first impactor and is close to its maximum displacement in the opposite direction to the impact direction, the second impactor generates less delamination, which is identified as destructive damage.

In this state, the surplus energy from the second impactor is transformed into elastic energy, which drives the plate back to its 0 displacement and then in the direction of impact. Between these two configurations, at a time lag of 0 ms, the displacements of the two impactors are uniform, and no particular damage state is generated (the difference in the delaminated surfaces in this case is directly linked to the distance of the impact centers from the edges of the plate). Constructive and destructive damage states are related to the displacement of the second point of impact. Indeed, if the displacements are additive in the same direction, a constructive damage state will occur. In the opposite case, where the displacements are in opposite directions, the sustaining of the displacements leads to a destructive damage state for the second impact. This highlights the crucial role played by the time lag, which, in most configurations, results in a larger total delaminated area than in the case of a single impact.

Following the delaminated surface caused by the second impactor, it was observed that constructive displacement leads to a larger delaminated surface, whereas destructive displacement results in a smaller delaminated surface. This phenomenon can be attributed to the conversion of the ball's kinetic energy into elastic energy. However, as the displacement approaches its maximum value, less energy can be stored elastically, and a higher proportion of energy is dissipated, leading to increased damage. No significant difference was noticed in the delamination created by the first impactor, as the ball generally reaches its maximum load at around 0.21 ms. To check whether there is a change in the delaminated surface of the second impactor when the time lag between the two impactors is less than 0.21 ms, the previously mentioned calculation with this particular time lag of 0.21 ms, corresponding to the time to reach the maximum force of the first impact, is shown Figure 15 (as previously mentioned, the poor consideration of the fiber failure by the

DPM should distort the delamination simulation, and this point will be developed in the next paragraphs).

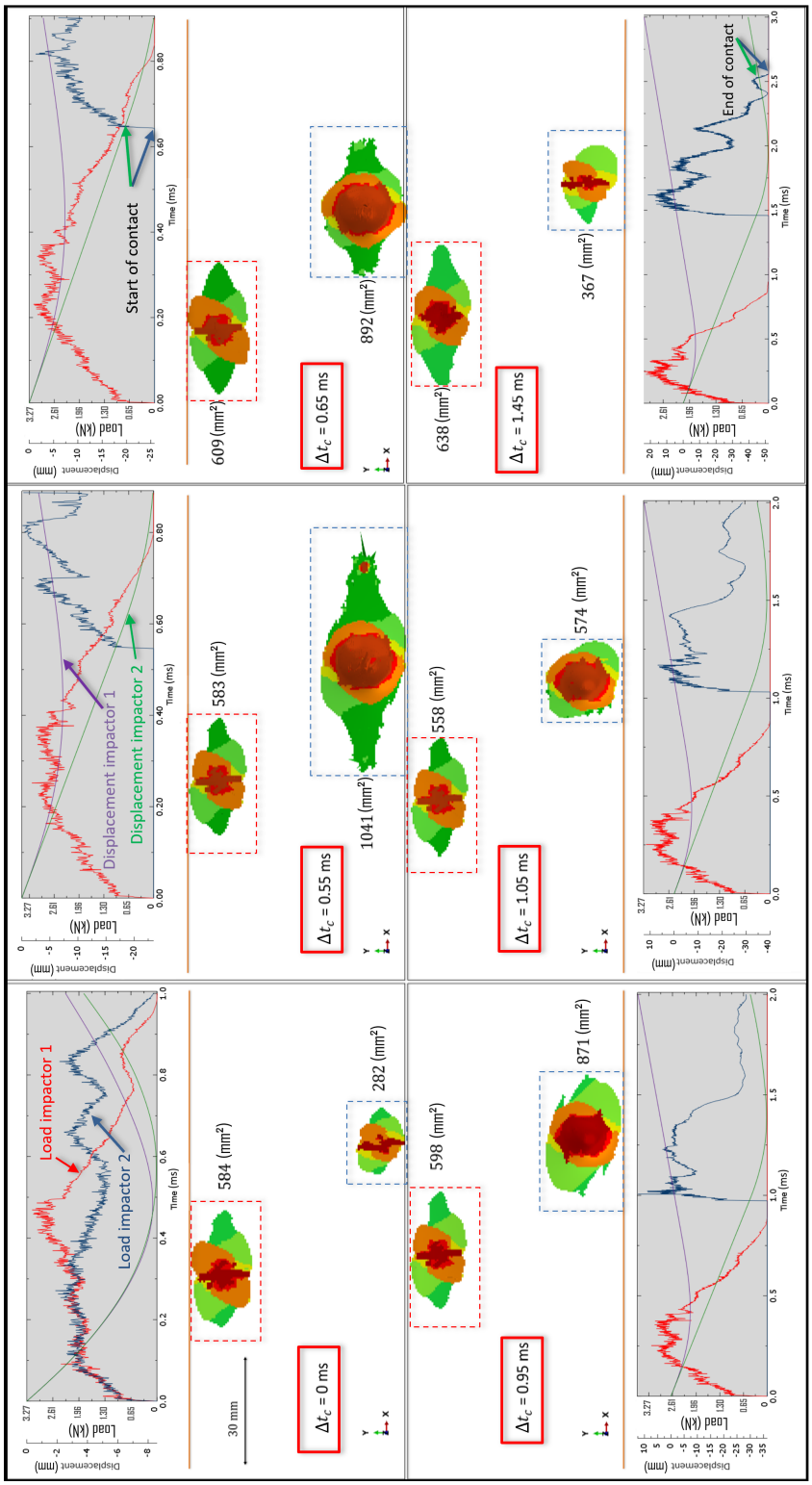

Figure 14. Effect of time lag on delaminated area (DPM).

It was concluded that this configuration is potentially the most dangerous, as the loading from the second impact is added to the maximum displacement generated by the first impactor. It was considered that the delamination caused by the second impact is actually much greater, but in the numerical model, an early fiber break occurred (which

significantly reduces the delaminated surface, as explained in configuration 30J/K/1). To account for this error, the ratio of the delaminated surface at the splinter level to the total delaminated surface in all C-scans conducted thus far was calculated. On average, over 50% of the delaminated surface originates solely from the splinter. This implies that, for the current configuration (Δt_c = 0.21 ms), the actual delaminated surface for the second impact can reach 1413 mm², resulting in a total delaminated surface of 2100 mm². This result confirms the same findings as those previously reported. Compared to this configuration (Δt_c = 0.21 ms), it was observed that the greater the time lag between the two impacts, the smaller the total delaminated area, as shown in Figure 16. It should be noted that the results of this figure are valid only for different values of Δt_c. For the case of two perfectly simultaneous impacts, it was observed that it does not follow the law announced in the figure since the displacements are homogeneous and do not produce any particular case of extreme loading, as shown in Figure 14 at Δt_c = 0 ms.

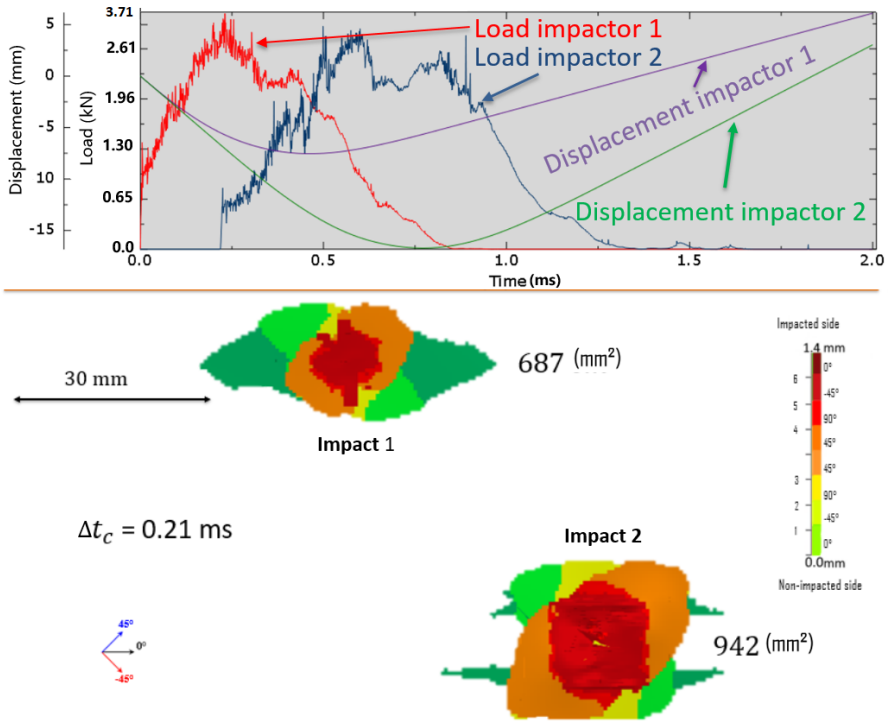

Figure 15. Effect of time lag on delaminated area (Δt_c = 0.21 ms).

Finally, it appears that the time lag between the start of the impactor movements is an essential parameter for multi-impacts. However, the time lag between the projectile/plate contact of two impacts is more crucial, as it accounts for two parameters simultaneously: the time lag between the start of the impactor movements and the plate vibration. Clearly, this depends on plate stiffness (thickness) and other impact parameters (energies, etc.), as demonstrated in configurations with a total energy of 30 J, where time lag and plate vibration are studied at low impact energies, and where Δt_c plays no role at very low energies.

It can be concluded that, for two simultaneous impacts, if the value of Δt_c is strictly greater than 0 and less than 0.21 ms (which corresponds to the maximum effort in the case of a single impact), the more the two impacts are delayed in time, the greater the delaminated surface due to the second impactor. If Δt_c is strictly greater than 0.21 ms and less than 1 ms, the more two impacts are delayed in time, the smaller the delaminated area, as shown in Figure 16. This principle is repeated throughout the vibration of the plate, so the results in the figure can be questioned for further study (to investigate whether the results regarding the timing of the second impact relative to the moment of maximum force

during the first impact remain valid when varying the characteristic parameters of the impactor and the impacted structure); see Figure 12, where two simultaneous impacts may behave similarly to two single impacts if the distance between them is sufficiently large. For perfectly simultaneous impacts, and the second impactor generates the least delaminated surface. This statement is valid only for the same distance between two impacts (or a distance of less than 160 mm in our case). If this condition is not met, the multi-impact character may not play an additional role, and the time lag between impacts may not result in any difference.

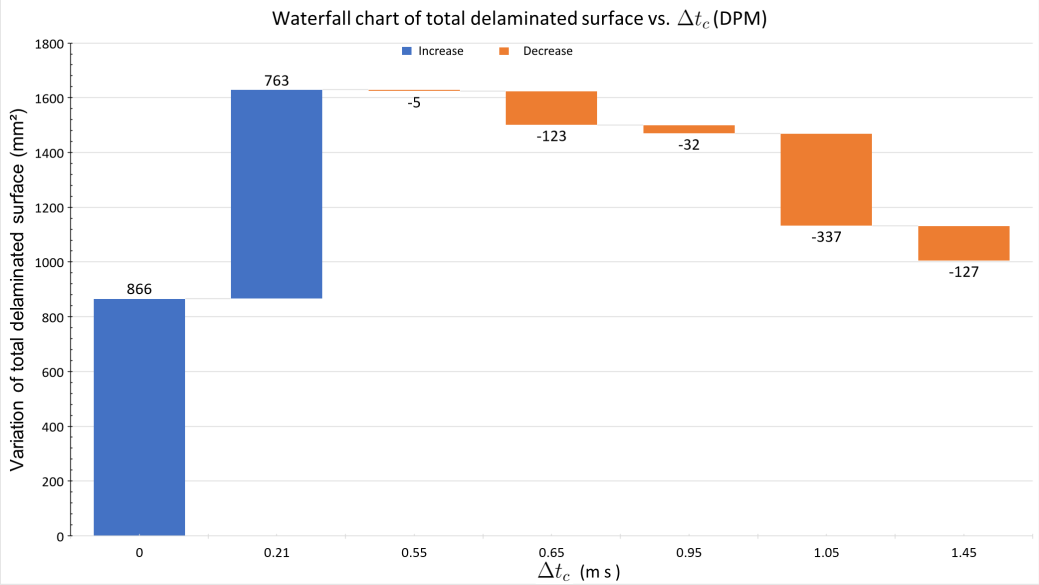

Figure 16. Variation of delaminated area as a function of time lag.

3.3. Simultaneous Impacts: Effect of the Number of Impacts

Mono-Impact and Two Simultaneous Impacts

As previously stated, it has been observed that impact damage varies according to factors such as the distance between impacts and impact energy. To study only the effect of the number of impacts, the positions of the impacts were set (see Figure 3), with 20 mm diameter balls at an energy of 15 J. In all experimental cases, the maximum time lag between the first and last ball arriving does not exceed 1 ms. The investigation was focused solely on the simultaneous configuration, which is considered more critical and original for comparison with single-impact cases.

As shown in Figure 17, the configurations 15J/M/2, and 30J/K/1 were used to minimize differences in impact parameters. It is observed that the case of a single impact is the most critical, with 30 J being dissipated instantaneously and locally on the composite structure (it is not totally dissipated, but energy is taken from the ball; after perforation, the ball must still retain residual kinetic energy). This is followed by two simultaneous impacts at a 22 mm distance in the 0° direction, where 15 J per ball is delivered (15J/M/2). This results in a shared delaminated surface between the two impacts (the union of the delaminated areas, not the sum), with the damage generated locally representing an impact at 15 J, which is naturally less significant than at 30 J and is also shared between the two impact zones. The large delaminated surface observed in the single-impact case is attributed to the phenomenon of interface 1 delamination during ball penetration, which is linked not only to matrix cracking but also to the direct contact between the ball and the last ply, leading to a more extensive tearing compared to delamination caused by matrix cracking alone. Next, a sequential case is added in position M, where only 15 J is dissipated instantaneously, resulting in less damage.

Finally, in the case of a mono-impact at 15 J, only 15 J can be dissipated in total, leading to the least amount of damage in the composite structure.

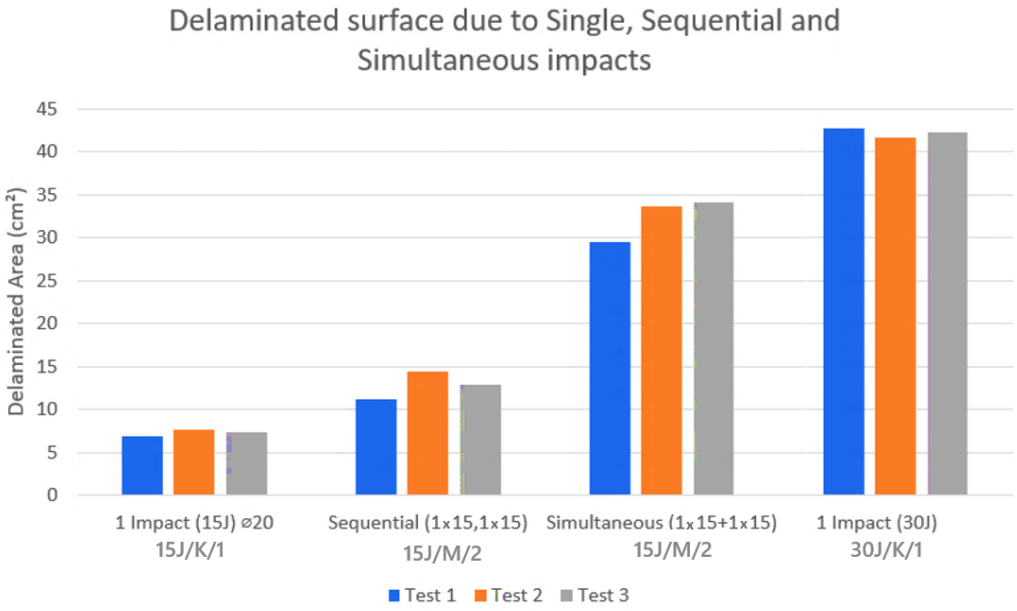

Figure 17. Delaminated area due to mono-impact, sequential, and simultaneous impacts.

4. Conclusions

In this study, the impact response of composite structures to quasi-simultaneous multi-impacts was thoroughly examined, addressing real-world scenarios such as hail, gravel, or external debris impacts. Experimental data were presented for various configurations. The results revealed that, beyond a certain distance between impacts, two simultaneous impacts effectively become equivalent to two mono-impacts. Moreover, a specific energy threshold per projectile was identified, beyond which the effect of multiple impacts becomes negligible, and the damage induced by each individual impact becomes more prominent. A key observation was the crucial role of the parameter Δt_c in multi-impact scenarios. Unlike mono-impact cases, where this parameter does not exist, Δt_c significantly influences the damage evolution and delamination patterns in multi-impact configurations. The analysis highlighted that shorter time intervals between impacts lead to more significant cumulative damage. This underscores the importance of considering the impact history and cumulative effects when assessing the long-term durability of composite materials under multi-impact loading conditions. This article provides experimental data on simultaneous multi-impacts that researchers could use to validate their models using a high-complexity problem. The findings emphasize the necessity of accounting for multi-impact effects in the design and assessment of composite materials used in environments prone to multiple simultaneous impacts.

Author Contributions: Conceptualization, A.S. and A.C.; methodology, A.S., C.B. and A.C.; software, A.S. and C.B.; validation, A.S. and C.B.; formal analysis, A.S., C.B. and A.C.; investigation, A.S. and C.B.; data curation, A.S. and C.B.; writing—original draft preparation, A.S.; writing—review and editing, A.S. and C.B.; visualization, A.S. and C.B.; supervision, A.S., C.B. and A.C.; project administration, A.C.; funding acquisition, C.B. and A.C. All authors have read and agreed to the published version of the manuscript.

Funding: This work was conducted at the DRIVE laboratory at ISAT in Nevers. This research was funded by the Bourgogne-Franche-Comté Region and the SPIM Doctoral School (ED37).

Institutional Review Board Statement: Not applicable.

Informed Consent Statement: Not applicable.

Data Availability Statement: The original contributions presented in this study are included in the article. Further inquiries can be directed to the corresponding authors.

Acknowledgments: We would like to thank the Clément Ader Institute (ICA, CNRS UMR 5312) for the use of the CALMIP computing facility.

Conflicts of Interest: The authors declare no conflicts of interest.

References

1. Cesari, F.; Dal Re, V.; Minak, G.; Zucchelli, A. Damage and residual strength of laminated carbon–epoxy composite circular plates loaded at the centre. *Compos. Part A Appl. Sci. Manuf.* **2007**, *38*, 1163–1172. [CrossRef]
2. Xiao-Yu, S.; Jian-Xin, T.; Zheng, H.; Xuan, G. A study on the failure mechanisms of composite laminates simultaneously impacted by two projectiles. *Adv. Compos. Lett.* **2018**, *27*, 96–106. [CrossRef]
3. Abrate, S. *Impact Engineering of Composite Structures*; CISM International Centre for Mechanical Sciences: Udine, Italy, 2011; pp. 97–128.
4. Wang, C.; Yew, C.H. Impact damage in composite laminates. *Comput. Struct.* **1990**, *37*, 967–982. [CrossRef]
5. Davies, G.A.O.; Olsson, R. Impact on composite structures. *Aeronaut. J.* **2004**, *108*, 541–563. [CrossRef]
6. Cantwell, W.J.; Worton, J. Comparison of the low and high velocity impact response of CFRP. *Compos. J.* **1989**, *20*, 545–551. [CrossRef]
7. Mokhtar, H.B. Contribution to the Study of Impact Damage on Composite Laminates: The Effect of Hygrothermal Ageing and Preloading. Ph.D Thesis, University of Burgundy, Dijon, France, 2012; pp. 78–85.
8. Amouzou, A.S.E.; Sicot, O.; Chettah, A.; Aivazzadeh, S. Experimental characterization of composite laminates under low-velocity multi-impact loading. *J. Compos. Mater.* **2019**, *53*, 2391–2405. [CrossRef]
9. Amaro, A.; Reis, P.; Moura, M.; Neto, M. Influence of multi-impacts on GRP composite laminates. *Compos. Part B* **2013**, *52*, 93–99. [CrossRef]
10. Bartus, S. Simultaneous and Sequential Multi-Site Impact Response of Composite Laminates. Ph.D. Thesis, University of Alabama at Birmingham, Birmingham, Alabama, 2006; p. 49.
11. Sultan, M.T.H.; Basri, S.; Rafie, A.S.M.; Mustapha, F.; Majid, D.L.; Ajir, M.R. High velocity impact damage analysis for glass epoxy laminated plates. *Adv. Mater. Res.* **2012**, *399–401*, 2318–2328. [CrossRef]
12. Rohrbach, Z.J.; Buresh, T.R.; Madsen, M.J. Modeling the exit velocity of a compressed air cannon. *Am. J. Phys.* **2012**, *80*, 24–26. [CrossRef]
13. Woojin, S.; Jihoon, K.; Kyeong, S.J.; Thi, T.G.L.; Jeonglae, K.; Dong, H.K.; Hyoungsoon, L.; Jaiyoung, R. Parametric study of a projectile launched by a compressed air cannon. *J. Mech. Sci. Technol.* **2023**, *37*, 5913–5933. [CrossRef]
14. Paredes-Gordillo, M.A.; Ivañez, I.; Garía-Castillo, S.K. Numerical study of the simultaneous multiple impact phenomenon on CFRP plates. *Compos. Struct.* **2023**, *320*, 117194. [CrossRef]
15. Rezasefat, M.; Beligni, A.; Sbarufatti, C.; Amico, S.C.; Manes, A. Experimental and Numerical Study of the Influence of Pre-Existing Impact Damage on the Low-Velocity Impact Response of CFRP Panels. *Materials* **2023**, *16*, 914. [CrossRef]
16. Kueh, A.B.H.; Sabah, S.H.A.; Qader, D.N.; Drahman, S.H.; Amran, M. Single and Repetitive Low-Velocity Impact Responses of Sandwich Composite Structures with Different Skin and Core Considerations: A Review. *Case Stud. Constr. Mater.* **2023**, *18*, e01908. [CrossRef]
17. Huo, L.; Kassapoglou, C.; Alderliesten, R.C. Influence of Neighbouring Damage on Delamination Growth in Multiple Indented Composites. *Mater. Des.* **2023**, *227*, 111723. [CrossRef]
18. Deka, L.J.; Bartus, S.D.; Vaidya, U.K. Multi-Site Impact Response of S2-Glass/Epoxy Composite Laminates. *Compos. Sci. Technol.* **2009**, *69*, 725–735. [CrossRef]
19. Vaidya, U.K.; Deka, L.J. Single and Multisite Impact Response of S2-Glass/Epoxy Balsa Wood Core Sandwich Composites. In *Major Accomplishments in Composite Materials and Sandwich Structures*; Springer: Dordrecht, The Netherlands, 2009; pp. 541–569.
20. Garzon-Hernandez, S.; Garcia-Gonzalez, D.; Arias, A. Multi-Impact Mechanical Behaviour of Short Fibre Reinforced Composites. *Compos. Struct.* **2018**, *202*, 241–252. [CrossRef]
21. Jackson, M.; Shukla, A. Performance of sandwich composites subjected to sequential impact and air blast loading. *Compos. Part B* **2011**, *42*, 155–166. [CrossRef]
22. Deka, L.J.; Bartus, S.D.; Vaidya, U.K. Numerical modeling of simultaneous and sequential multi-site impact response of S-2 glass/epoxy composite laminates. In *Composites & Polycon*; American Composites Manufacturers Association: Tampa, FL, USA, 2007.

23. Hall, Z.E.C.; Liu, J.; Brooks, R.A.; Liu, H.; Dear, J.P. Impact testing on the pristine and repaired composite materials for aerostructures. *Appl. Mech.* **2023**, *4*, 421–444. [CrossRef]
24. Safri, S.N.A.; Sultan, M.T.H.; Yidris, N.; Mustapha, F. Low velocity and high velocity impact test on composite materials—A review. *Int. J. Eng. Sci.* **2014**, *3*, 50–60.
25. Costa, U.O.; Nascimento, L.F.C.; Garcia, J.M.; Bezerra, W.B.A.; Monteiro, S.N. Evaluation of Izod impact and bend properties of epoxy composites reinforced with mallow fibers. *J. Mater. Res. Technol.* **2020**, *9*, 373–382. [CrossRef]
26. Hufenbach, W.; Ibraim, F.M.; Langkamp, A.; Böhm, R.; Hornig, A. Charpy impact tests on composite structures—An experimental and numerical investigation. *Compos. Sci. Technol.* **2008**, *68*, 2391–2400. [CrossRef]
27. Sfarra, S.; Ibarra-Castanedo, C.; Santulli, C.; Paoletti, A.; Paoletti, D.; Sarasini, F.; Bendada, A.; Maldague, X. Falling weight impacted glass and basalt fibre woven composites inspected using non-destructive techniques. *Compos. Part B Eng.* **2013**, *45*, 601–608. [CrossRef]
28. V.; erKlok, A.; Stamm, A.; Dorer, J.; Eryi, H.; Auvenshine, M.; Pereira, J.M.; Xiao, X. An experimental investigation into the high velocity impact responses of S2-glass/SC15 epoxy composite panels with a gas gun. *Int. J. Impact Eng.* **2018**, *111*, 244–254. [CrossRef]
29. Deconinck, P. Étude du Comportement à L'Impact de MatéRiaux Composites RenforcéS par Tufting. Ph.D Dissertation, University of Lorraine, Nancy, France, 2014; pp. 13–16.
30. Gama, B.A.; Lopatnikov, S.L.; Gillespie, J.W., Jr. Hopkinson bar experimental technique: A critical review. *Appl. Mech. Rev.* **2004**, *57*, 223–250. [CrossRef]
31. Lamberson, L. Investigations of high-performance fiberglass impact using a combustionless two-stage light-gas gun. *Procedia Eng.* **2015**, *103*, 341–348. [CrossRef]
32. Zhou, H.; Jing, K.; Xie, S.; Feng, Z.; Wang, H. Experiment of high-speed cumulative impact of carbon fiber plate based on air cannon. *Sci. Technol. Compos. Mater.* **2023**, *40*, 29–35.
33. Soufri, A.; Chettah, A.; Piezel, B.; Bouvet, C. A newly developed compressed air cannon test bench designed for multi-impact analysis of composite structures. *Appl. Mech.* **2024**, *5*, 997–1010. [CrossRef]
34. Soufri, A. Multi-Impact Behavior of Composite Structures: Experimental and Numerical Approach. Ph.D. Thesis, University of Burgundy, Dijon, France, 2023.
35. Gurit. SE 84LV: Epoxy-Based Prepreg Curing at Low Temperature (SE84LV-25-0519). 2007. Available online: https://www.gurit.com/ (accessed on 8 December 2024).
36. Ravi, C.; Nistal, A.; Falzon, B.G.; Hawkins, S.C. Mode I Interlaminar Fracture Toughness of Carbon Nanotube Web-Modified Polymer Composites. In Proceedings of the 21st International Conference on Composite Materials (ICCM21), Xi'an, China, 20–25 August 2017.
37. Falzon, B.G.; Hawkins, S.C.; Huynh, C.P.; Radjef, R.; Brown, C. An investigation of Mode I and Mode II fracture toughness enhancement using aligned carbon nanotubes forests at the crack interface. *Compos. Struct.* **2013**, *106*, 65–73. [CrossRef]
38. Leonardo, S.D.; Nistal, A.; Catalanotti, G.; Hawkins, S.C.; Falzon, B.G. Mode I interlaminar fracture toughness of thin-ply laminates with CNT webs at the crack interface. *Compos. Struct.* **2019**, *225*, 111178. [CrossRef]
39. Bouvet, C.; Castanie, B.; Bizeul, M.; Barrau, J.J. Low velocity impact modelling in laminate composite panels with discrete interface elements. *Int. J. Solids Struct.* **2009**, *46*, 3820–3836. [CrossRef]

Disclaimer/Publisher's Note: The statements, opinions and data contained in all publications are solely those of the individual author(s) and contributor(s) and not of MDPI and/or the editor(s). MDPI and/or the editor(s) disclaim responsibility for any injury to people or property resulting from any ideas, methods, instructions or products referred to in the content.